Tissue adhesive hydrogel based on Upcycled Proteins and Plant Polyphenols for Enhanced Wound Healing

Hafez Jafari[1*], Pejman Ghaffari-Bohlouli[1], Mohsen Alishahi[2], Farideh Davani[3], Seyyed Sajad Daneshi[4], Reza Heidari[5], Mohammad Hossein Morowvat[5] Seyyed Vahid Niknezhad[6*], Lei Nie[*7], Houman Savoji[8,9,10*], Amin Shavandi[1*]

[1] BioMatter Unit—BTL, École Polytechnique de Bruxelles, Université Libre de Bruxelles, Avenue F.D. Roosevelt, 50-CP 165/61, Brussels 1050, Belgium,

[2] Burn and Wound Healing Research Center, Shiraz University of Medical Sciences, Shiraz, 71345-1978, Iran

[3] Fiber Science Program, Department of Human Centered Design, College of Human Ecology, Cornell University Ithaca, NY 14853, USA

[4] Histomorphometry and Stereology Research Center, Shiraz University of Medical Sciences, Shiraz, Iran

[5] Pharmaceutical Sciences Research Center, Shiraz University of Medical Sciences, Shiraz, Iran

[6] Department of Cell and Tissue Biology, University of California, 513 Parnassus Avenue, San Francisco, CA 94143, USA

[7]College of Life Sciences, Xinyang Normal University, Xinyang 464000, PR China

[8] Institute of Biomedical Engineering, Department of Pharmacology and Physiology, Faculty of Medicine, University of Montreal, Montreal, QC, H3T 1J4, Canada

[9] Research Center, Centre Hospitalier Universitaire Sainte-Justine, Montreal, QC, H3T 1C5, Canada

[10] Montreal TransMedTech Institute, Montreal, QC, H3T 1J4, Canada

Abstract

This study investigates the potential of keratin and silk as natural structural proteins for designing tissue adhesives for wound healing. The study demonstrates the silk-wool-tannic acid (SF-Wool-TA) complex as an *in situ* tissue adhesive through the utilization of polyphenol chemistry. Keratin is first isolated from coarse sheep wool using a green microwave treatment process. Due to the presence of functional groups such as tyrosine, carboxyl, and thiol groups; silk, and keratin can form multiple interactions with pyrogallol and catechol functional groups of TA to form an *in situ* adhesive hydrogel. The SF-Wool-TA hydrogel exhibits in situ gelation, recyclability, moldability, elasticity (G'>100 kPa), adhesiveness, self-healing properties, 3D printability, antibacterial activity, antioxidant properties, and biocompatibility. The inclusion of wool keratin also enhances the hydrophilicity of the hydrogel. The hydrogel was tested *in vivo* and enhanced wound healing in a full-thickness skin incision model. The keratin-polyphenol interaction represents an attractive hybrid material for advanced biomaterials applications, particularly in the field of skin wound healing.

Keywords: Wool keratin; Tannic acid; Silk fibroin; Tissue adhesive, Wound healing

1. Introduction

Animal by-products such as bones, hides, wool, and feathers are rich sources of protein that, if not correctly recycled or disposed of, can adversely impact the environment. In the EU alone, over 20 million tons of animal by-products annually emerge from slaughterhouses and food plants [1]. Using this waste to develop valuable products is a key pillar of a green and circular economy. Animal-based proteins, such as collagen, gelatin, silk, elastin, and keratin, constitute an essential class of biopolymers that have been exploited in biomedical engineering [2-6]. In this context, the valorization of animal by-products offers sustainability and economic development in several sectors, including the biomedical and pharmaceutical industries, as well as developing biomaterials for human health, such as wound healing, tissue engineering, biosensing, and tissue adhesives. Recently, the development of tissue sealants and adhesives has become popular as a greener alternative to sutures and staples for wound healing applications [7]. Tissue adhesives can overcome traditional suturing limitations such as the chance of bacterial infection [8], fragile tissue damage [9], lack of efficacy in emergencies, and minimally invasive approaches [7].

An ideal tissue adhesive should possess biocompatibility, wet adhesion, high mechanical stability, and ease of storability for emergencies [10]. Moreover, adhesives with self-healing and injectability are required for applications under dynamic forces via a minimally invasive approach [11]. Besides, the hemostatic activity of tissue adhesive materials plays a crucial role in acute clinical demand, such as arterial and venous bleeding wounds [12]. Several materials and chemistry have been utilized for the development of tissue adhesives such as cyanoacrylates [13], polyethylene glycol-based [14], and poly(glycerol sebacate) acrylate[15] as synthetic tissue adhesives; alternatively, fibrin [16], gelatin [17,18], and polysaccharides[19], as biological tissue adhesives materials. However, only a few have received clinical approval due to the challenges during the transition, particularly inadequate adhesiveness in wet conditions under dynamic forces [7].

Bombyx mori silk fibroin (SF) is a natural protein derived from *Bombyx mori (B. mori)* domestic silkworms containing a core protein fibroin (72-81%) and its glue-like coating sericin (19-28%) [20,21]. SF is a promising candidate for the design of tissue adhesives due to the presence of multiple functional

groups such as amines, carboxyl, alcohols, and thiols, endowing SF with multiple interactions for hydrogel formation [22,23]. Recent studies showed a fast and facile preparation of adhesives based on SF and tannic acid (TA) as a plant polyphenol [24-26]. TA with inherent antioxidant, antibacterial, and anti-inflammatory exhibited high affinity to SF due to the formation of multiple interactions such as hydrogen bonding, hydrophobic, and electrostatic interaction, as well as van der Waals forces resulting in the formation of *in situ* adhesive hydrogel [27,28]. Wool-based keratin, as another protein-based animal by-product, has exhibited high cellular attachment and proliferation due to the presence of different cell binding sites such as arginine-glycine-aspartic acid (RGD), leucine–aspartate–valine (LDV), as well as glutamic acid–serine (EDS) [29]. Furthermore, due to the presence of functional groups such as amino, carboxyl, and thiol groups, keratin can form multiple interactions with TA for biomedical hydrogel formation [30]. In this study, we proposed a facile and effective method for developing *is situ* tissue adhesive with flexibility, and bioactivity using animal protein rich materials such as SF and wool keratin crosslinked by TA as a plant polyphenol.

2. Result and discussion

2.1. Hydrogel formation

The hydrogel formation process is illustrated in Fig 1A. First, aqueous SF solution (5 wt%) was prepared from *B. mori cocoons*; afterward, the prepared wool keratin powder (5 wt%) was added to the SF solution. The adhesive SF-Wool-TA was immediately formed upon adding TA solution to the wool-containing SF solution (Video S1) due to the formation of multiple non-covalent interactions between TA molecules, SF, and wool keratin [31]. The gelation mechanism between SF and TA primarily results from the synergy of hydrophobic and hydrogen bonding of polyphenol with protein, particularly the high affinity of TA to the hydrophobic region in SF and the keratin.[27] After mixing TA and SF-wool keratin solution, the initial attraction and attachment are due to the van der Waals forces (Lennard-Jones potential energy). After that, electrostatic forces gradually increase and become dominant[28]. Hydrophobic bonding is the reason for the entry of TA into hydrophobic regions of SF and keratin, and reinforces the first stage association via the subsequent hydrogen bonding between amino groups, carboxyl groups of SF, and keratin protein with phenolic hydroxyl groups of TA [24,30]. Therefore, the

synergy of non-covalent interactions resulted in a rapid formation of adhesive hydrogel (Scheme 1). TA may induce the conformational transition of SF and keratin protein from random coil to β-sheet conformation which can assist the hydrogel formation [28]. Moreover, the freeze-dried adhesive hydrogel powder exhibited a fast self-gelling upon mixing the water droplet with the powder without needing external stimuli or a crosslinker (Fig 1A), which can have the potential for clinical use as a self-gelling powder at the defect site [32].

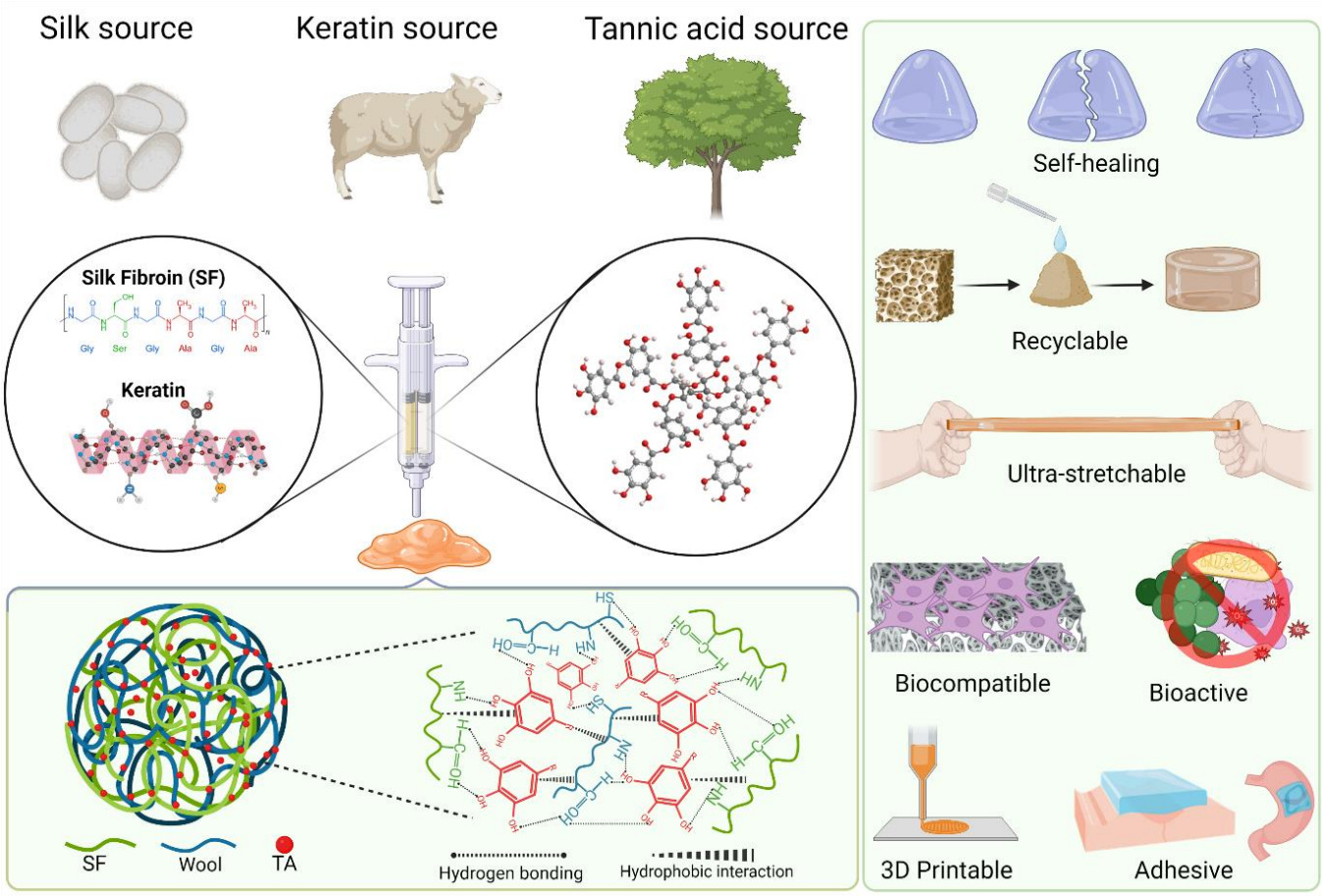

Scheme 1. Schematic illustration of silk fibroin (SF), wool-keratin, and tannic acid (TA) sources and structure, as well the possible interactions between SF, wool, and TA in the SF-Wool-TA hydrogel and the various hydrogel unique properties.

The possible interaction and chemical composition of SF-Wool-TA hydrogel were determined using FTIR analysis (Fig 1C). Pure TA spectrum exhibited characteristic peaks attributed to stretching vibration of the phenolic hydroxyl (-OH), C=O groups of carboxylic ester, aromatic C=C stretch, the substituted benzene ring vibration, and bending aromatic vibration C–H groups at 3312, 1698, 1614-

1443, 1183-1120, and 757 cm^{-1}, respectively [33]. Also, the pure SF spectrum exhibited a characteristic peak of C=O stretching vibrations of the amide I group at 1626 cm^{-1} and C-O stretching vibrations of Amide II at 1523 cm^{-1}. Similar to the SF spectrum, pure wool keratin showed a characteristic peak of N–H stretching (Amide A) at 3273 cm^{-1}, C=O bond (Amide I) at 1640 cm^{-1}, and C-N and C-O stretching vibrations (Amide II) at 1540, indicating the rich keratin structure of the wool keratin [34,35]. The SF-TA and SF-Wool-TA hydrogel spectra exhibited similar peaks to the TA spectrum showing the presence of TA incorporated into the hydrogel. However, the hydroxyl groups of TA (3312 cm^{-1}) were shifted to the lower wavenumber in the spectra of SF-TA (3291 cm^{-1}) and SF-Wool-TA (3285 cm^{-1}), revealing the formation of hydrogen bonding between hydroxyl groups of TA with SF and keratin in wool [24]. Furthermore, the peak attributed to the C=O stretch vibration of TA (1698 cm^{-1}) was shifted to 1644 cm^{-1} in the SF-TA, and SF-Wool-TA spectra, as a result of interaction between the hydrogen donor hydroxyl groups of TA, leading to an increase in the vibrational energy of C=O bonding. The shifting in the wavelength is in agreement with the previous result indicating the hydrogen bonding between SF and keratin with TA [30,31]. Moreover, the Amide I and Amide II peaks of SF and wool keratin were shifted to 1609 and 1513 cm^{-1} after the hydrogel formation.

The crystalline structure of hydrogels was investigated using an X-ray diffractometer (XRD) pattern (Fig 1C). Wool keratin showed the α-helix and β-sheet structure according to the peaks presented at 9° and 19°, respectively [36]. However, after the interaction with TA, the peak attributed to the α-helix structure of wool keratin disappeared in the SF-Wool-TA hydrogel spectrum, and the β-sheet structure peak intensified, indicating the conformational transition of protein structure confirming the FTIR result.

2.2. Physiochemical characterization of the adhesive hydrogels

First, the microstructure of freeze-dried hydrogels was investigated using SEM (Fig 1D). Both hydrogels exhibited a heterogenous three-dimensional porous microstructure favorable for cell proliferation and growth [37]. However, SF-TA hydrogels exhibited a denser microstructure with smaller pore sizes than the SF-Wool-TA hydrogel, possibly due to the higher crosslinker density in the SF-TA hydrogel. Upon investigation of the initial water, and gel content of hydrogels (Fig 1E and 1F), it was

observed that the SF-Wool-TA hydrogel had a slightly higher water and gel content than the SF-TA hydrogel. This difference in water content could be attributed to the increased porosity of the SF-Wool-TA hydrogel and the intrinsic hydrophilicity of wool keratin, which enables it to adsorb moisture [38]. The swelling property of a gel is important for drug loading, releasing, and wound exudate absorption, which can enhance the hemostasis rate [39]. Swelling and water uptake depend on the hydrophilic network, porous structure, and osmotic pressure difference between the gel and the environment [40]. To evaluate water absorption capacity and the impact of wool keratin polar groups, we studied the swelling of SF-TA and SF-Wool-TA hydrogels. Swelling occurred in three steps (Fig 1G): (1) rapid absorption in less than 2 hours, (2) decreased uptake ratio from 2 to 48 hours, increasing from ~ 56.4% to ~ 198.0% for SF-Wool-TA and from ~ 46.4% to ~ 122.2% for SF-TA, and (3) slight increase in swelling after 48 hours. SF-Wool-TA gel had ~ 90% higher ultimate water uptake than the SF-TA hydrogel (Fig 1G). Hence, it can be concluded that wool keratin increases the hydrophilic groups in the system [38,41,42]. Moisture in wounds improves the re-epithelialization rate by facilitating epithelial cell movement [43]. Hydrogel's water evaporation rate is critical in maintaining wound moisture. Water retention in SF-TA and SF-Wool-TA was assessed using the swollen hydrogel water retention assay [40]. As shown in Fig 1H, both hydrogels lost moisture over time, but SF-Wool-TA lost half its water (from 188 ± 3.5% to 96 ± 4%) within 3 hours, while SF-TA lost less moisture in the same period. Rapid water evaporation in the swollen hydrogels causes free water molecule evaporation[40]. Half-bounded water molecules evaporated slowly until 48h with the remaining bounded water molecules retained in the hydrogel network beyond 72 hours. Although SF-Wool-TA hydrogel had higher water uptake, they also had higher water retention due to more free water molecule absorption. Both samples had the same reduction rate after initial water evaporation. The TA release from the hydrogels was investigated using UV spectrophotometry (Fig 1I). Both hydrogels released TA at a similar rate, but there was a slight difference up to 12 hours after being placed in PBS (pH 7.4) at 37°C. This may be due to excess TA being trapped or loosely bound within the network. A sustained TA release rate was observed between 12 h to 72 h. The SF-Wool-TA hydrogel exhibited a higher ultimate TA release (2994.3 ± 163.8 ppm) compared to the SF-TA hydrogel (2421.23 ± 187.1 ppm) after 144 h, possibly due to the higher amount of TA loaded into the SF-Wool-TA hydrogel.

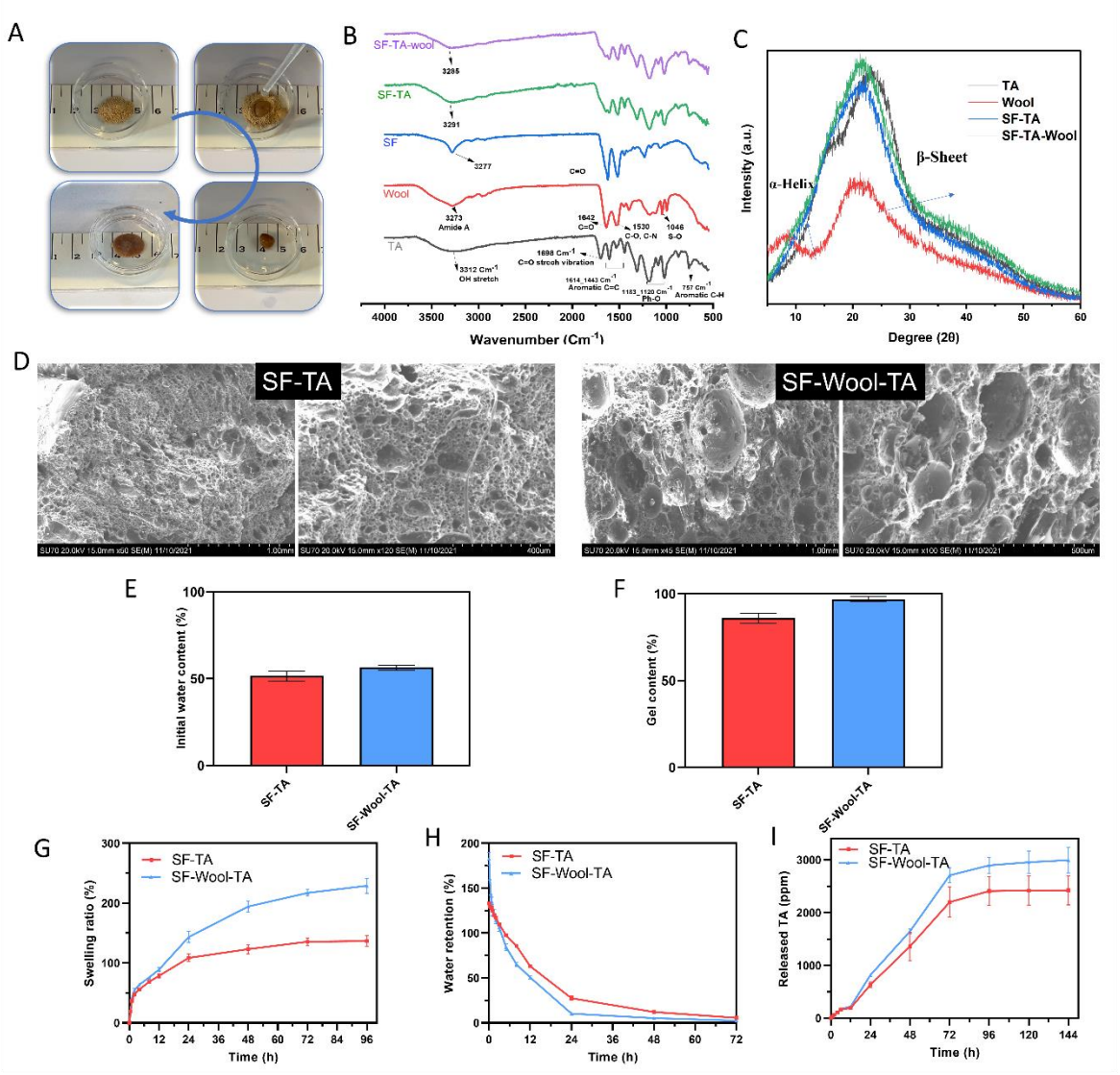

Fig 1. (A) The self-gelling properties of the SF-Wool-TA hydrogel by forming the gel immediately after the addition of a water droplet to the freeze-dried hydrogel powder; (B) FTIR spectra of SF, TA, wool, SF-TA hydrogel, and SF-Wool-TA hydrogel; (C) XRD pattern of TA, Wool, SF-TA, and SF-Wool-TA; (D) microstructure of SF-TA and SF-Wool-TA hydrogels; (E) Initial water content of the hydrogels; (F) Gel content of the hydrogels; (G) swelling ratio of the hydrogels; (H) Water retention rate of the hydrogels; (I); Amount of TA released from the hydrogel in PBS.

2.3. Viscoelastic and self-healing properties

The viscoelastic properties of SF-TA and SF-Wool-TA hydrogel were investigated using oscillatory tests (Fig 2). Both SF-TA (Fig 2A) and SF-Wool-TA (Fig 2B) hydrogels showed time-dependent properties, with a sol-like behaviour for the first 5 min and a transition to gel-like behavior thereafter,

indicated by an increase in G' and G" and their crossing point. By 10 min, the G' of SF-TA and SF-Wool-TA mixtures increased due to the dehydration leading to increased stiffness and elasticity. The dynamic viscosity results (Fig 2C) showed that the hydrogels had shear-thinning behavior showing the injectability of the hydrogel [44]. Frequency-dependent viscoelastic properties of hydrogels were evaluated to ensure the self-stiffness of hydrogels on the fresh samples (Fig 2D) and by 10 min (Fig 2E).

The hydrogels exhibited a solid-like behavior by 10 min, confirming the time sweep test results indicating the self-solidification of the hydrogels. By increasing frequency (0.1 to 100 Hz)m G' of both hydrogels significantly increased (from 75 and 21 kPa to 394 and 184 kPa). This can be due to dynamic non-covalent interactions (hydrogen bonding) restricting polymer chain movement at high frequency [33,45]. The amplitude sweep test identified a narrow linear viscoelastic region (LVR) of less than 5% with a critical strain of 59% and 46% for SF-TA and SF-Wool-TA hydrogels, respectively (Fig 2F). Overall, the addition of wool keratin to the SF-TA hydrogel decreased the stiffness of the hydrogel.

Furthermore, the self-healing performance of adhesive hydrogels was evaluated. The adhesive hydrogel (SF-Wool-TA) exhibited immediate self-healing after contacting two pieces of hydrogels and could withstand a certain stretch (Fig 2G) due to the presence of dynamic non-covalent interactions (hydrogen bonding and hydrophobic interaction) between SF, wool, and TA molecules which can undergo a fast re-construction after the external damage[26]. The dynamic non-covalent interactions present within the hydrogels allowed for their self-gelling behavior as freeze-dried hydrogel powder and contributed to the fast self-healing behavior after cutting and contacting the two pieces of hydrogels (Fig 2H).

The self-healing properties were evaluated using a step-strain sweep test, which showed rapid self-healing for both SF-TA (Fig 2I) and SF-Wool-TA (Fig 2J) hydrogels. Upon reaching a high strain step (500%), the hydrogels exhibited sol-like behavior (G" > G'). However, upon returning to the initial strain step (1%), the hydrogels recovered 100% of their original G', demonstrating their immediate self-healing properties.

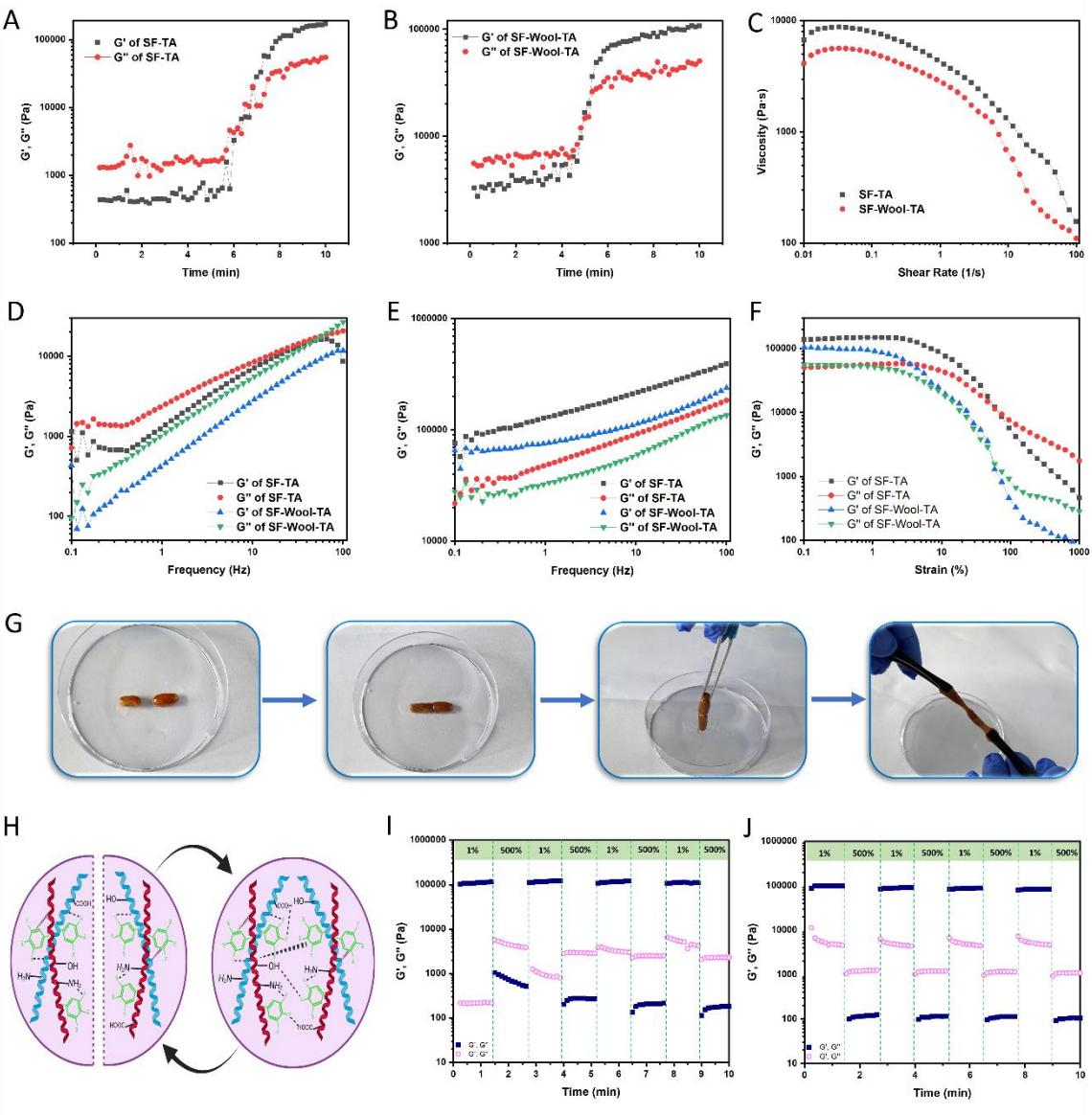

Fig 2. Viscoelastic and self-healing properties of adhesive hydrogels. (A) Time dependant storage (G') and loss (G'') moduli of SF-TA hydrogel; (B) Time dependant storage (G') and loss (G'') moduli of SF-Wool-TA hydrogel; (C) Flow curve of SF-TA and SF-Wool-TA hydrogels; (D) Frequency dependant G' and G'' of SF-TA, and SF-Wool-TA hydrogels at t=0; (E) Frequency dependant G' and G'' of SF-TA, and SF-Wool-TA hydrogels at t=10 (after solidification); (F) Amplitude sweep test of SF-TA, and SF-Wool-TA hydrogels at t=10 (after solidification); (G) Macroscopic observation of SF-Wool-TA self-healing properties; (H) Self-healing mechanism of the hydrogels; (I) G' and G'' of SF-TA hydrogel under the step-strain sweep test; (I) G' and G'' of SF-Wool-TA hydrogel under the step-strain sweep test.

2.4. Mechanical properties and 3D printability

The mechanical properties and the stretchability of SF-TA and SF-Wool-TA hydrogels were evaluated using a universal tensile testing machine (Figs 3 A, B), and the hydrogels tensile stress (Fig 3D), strain (Fig 3E), and Young modulus (Fig 3F) were recorded. Both hydrogels showed stretchability up to 20 times their initial length (Fig 3C). The SF-Wool-TA demonstrated a lower tensile stress compared to SF-TA hydrogel (Fig 3D), while the elongation at break increased after the wool keratin addition, possibly due to the softening impact of the wool keratin on the hydrogel. Moreover, the Young modulus of the hydrogel decreased from 6.1 ± 0.8 to 4.9 ± 0.6 after the wool keratin incorporation (Fig 3F).

Furthermore, the SF-Wool-TA hydrogel 3D printability for developing customized adhesive hydrogels was evaluated using a 3D printing system (BioScaffolder 3.2, GeSiM, Germany) (Fig 3G). The SF-Wool-TA could be easily extruded through an extrusion nuzzle (18 G) in response to shear force. Besides, the extruded hydrogel could retain its initial structure due to the dynamic nature of the non-covalent bonding presented in the hydrogel. The effect of printing pressure (150-200 kPa) was investigated on the printability of the hydrogel (Video S2), and 160 kPa was used to perform the 3D printing at a speed of 10 $mm.s^{-1}$ and 37 ^{o}C. Moreover, in addition to extrudability, the SF-Wool-TA showed moldability (Fig H).

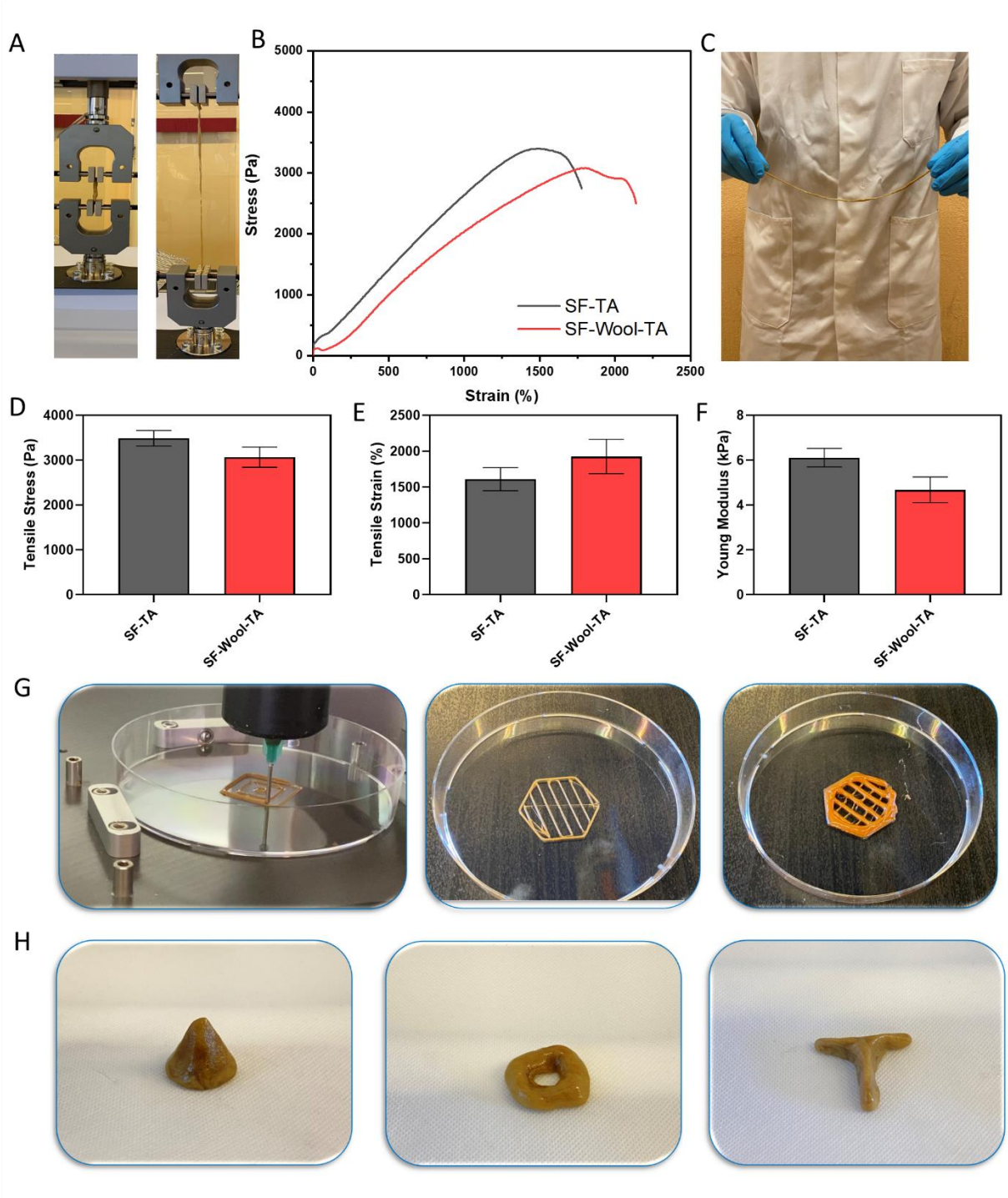

Fig 3. Mechanical properties, 3D printability, and moldability of adhesive hydrogel; (A) Tensile testing photograph of the hydrogels; (B) Tensile stress-strain curves of adhesive hydrogels; (C) Stretchability of the SF-Wool-TA hydrogel; (D) Maxim tensile stress of SF-TA, and SF-Wool-TA hydrogels; (E) Tensile strain of SF-TA, and SF-Wool-TA hydrogels; (F) Young modulus of SF-TA, and SF-Wool-TA

hydrogels; (G) 3D printability of the SF-Wool-TA hydrogel; (H) Moldability of the SF-Wool-TA hydrogel.

2.5. Adhesion properties of hydrogels

The adhesion performance of SF-TA and SF-Wool-TA hydrogels was evaluated on the porcine skin using the lap shear test (Fig 4A) by measuring the maximum shear adhesion after the detachment. The presence of rich catechol groups of TA in the hydrogels provided the hydrogels with high and repeatable adhesiveness to different substrates such as plastic, stain steel, glass, as well as biological tissues (rat heart, and kidney), indicating the adhesiveness of hydrogels to the various substrate (Fig 4B). Moreover, the hydrogels exhibited ability to preventing water leakage (Fig 4B, Video S3) as well as adhesiveness under wet conditions (Video S4). The adhesiveness of the hydrogels is due to the presence of hydroxyl groups (25 in each TA molecule) which endows the hydrogels with the formation of strong hydrogen bonding within the various substrate, including metal, wood, glass, and biological tissues [26,28]. Moreover, TA can form other interactions with substrates, such as H-bonding, π-π stacking, hydrophobic interaction with wood, or metal coordination interaction with metallic substrates[33]. Moreover, the interaction between amino and thiol groups of peptides in biological tissues with TA is accountable for the adhesiveness of TA-based hydrogels to biological tissue (Fig 4I) [46]. Moreover, the Van der Waals interactions between TA and amino acids such as Gly, Ala, and Ser, as well π–π stacking of TA with amino acids' rigid planar structures, can play a critical role in the adhesion of hydrogels to biological tissues[28].

The lap shear test results (Figs 4C, F) showed higher adhesive strength for SF-Wool-TA hydrogel (96.2 ± 14.3 kPa) compared to the SF-TA (70.6 ± 11.1 kPa) hydrogel. Moreover, both hydrogels showed a repeatable adhesion to the porcine skin. SF-TA hydrogel adhesion was significantly decreased after each repeat (Figs 4D, G), while there was no significant between repeated adhesion tests of SF-Wool-TA hydrogel (Figs 4E, F). The results showed that wool keratin incorporation increased the hydrogels' adhesion strength and improved the efficacy of cyclic adhesion of the hydrogel. This phenomenon could be due to the higher loading of TA into SF-Wool-TA compared to the SF-TA hydrogel since the adhesion of TA-based hydrogels to biological tissue relies on the presence of free catechol groups in

the hydrogels [24]. Moreover, previous studies reported that keratin protein could increase tissue adhesiveness like other proteins such as gelatin and elastin[47,48].

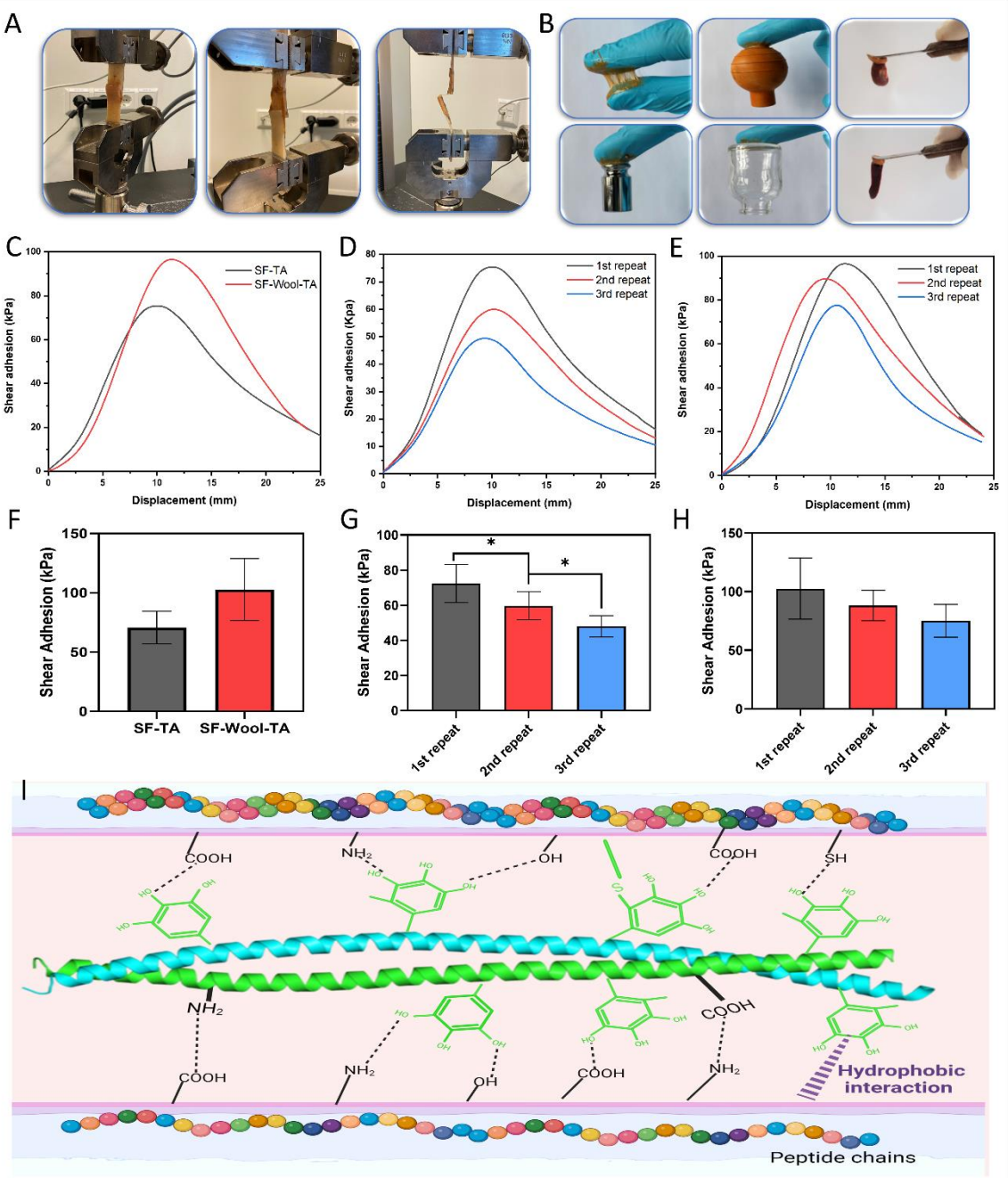

Fig 4. The adhesion performance of SF-TA and SF-Wool-TA hydrogels. (A) Photographs of the Lap shear test process using porcine skin; (B) Adhesive performance of the hydrogels with different substrates, including plastic, stainless steel, glass, and biological tissues, as well as the waterproof properties of the adhesive; (C) Lap shear stress-displacement curves for SF-TA and SF-Wool-TA adhesives; (D) The repeated Lap shear stress-displacement curves SF-TA hydrogels; (E) The repeated Lap shear stress-displacement curves SF-Wool-TA

hydrogels; (F) The adhesive strength of SF-TA and SF-Wool-TA hydrogels; (H) The repeated adhesive strength of SF-TA hydrogels; (G) The repeated adhesive strength of SF-Wool-TA hydrogels.; (I) The possible adhesiveness mechanism of SF-Wool-TA hydrogel to the biological tissue.

2.6. Hydrogels bioactivities

The DPPH scavenging assay was performed to determine the adhesive hydrogels' antioxidant capability (Fig 5A). The results revealed a high DPPH scavenging activity for both SF-TA (87.5 ± 4.6 %) and SF-Wool-TA (84.4 ± 3.3 %) without any significant difference between the hydrogels. Since the SF and wool keratin have not shown significant antioxidant activity [49], the presence of TA molecules is the primary reason for the antioxidant activity of the hydrogels. Due to the presence of multiple hydroxyl groups in the galloyl and catechol groups, TA can stabilize the delocalized electron contributing to the antioxidant activity of SF-TA and SF-Wool-TA hydrogels (Fig 5C) [50]. Moreover, the DPPH solution incubated with hydrogel samples was completely decolorized after 30 min indicating the complete DPPH radical reduction via electron pairing with hydrogen atoms in TA (Fig 5B).

The antibacterial activity of hydrogels was determined against the two most common colonized bacteria in chronic wound tissue, such as *Staphylococcus aureus (S. aureus)* and *Escherichia coli (E. coli)*, using disk diffusion and colony counting assay [51]. Both SF-TA, and SF-Wool-TA hydrogels showed a similar zone inhibition (5-6 mm) against *S. aureus* and *E. coli* without a significant difference (Fig 5D). According to previous works, silk and wool keratin do not show considerable antibacterial activity [31,52]. It can be concluded that the antibacterial effect of the hydrogels comes from TA [31,40], and since the TA release rate from SF-TS and SF-Wool-TA hydrogels was the same at the first 24 h, it is reasonable to show the same antibacterial activity. Furthermore, the colony counting assay (Fig 5D) revealed a similar antibacterial effect for both hydrogels; however, both hydrogels exhibited a significant antibacterial effect compared to the control sample against *E. coli* and *S. aureus*. Thus, both hydrogels with the potency to release TA in a controlled manner could prevent the growth of bacteria.

Moreover, the hydrogels' cytocompatibility was evaluated using MTS and Live/dead assay. MTS assay results (Fig 4E) revealed the non-toxicity of the hydrogels after 7 days of incubation with 3T3-L1 cells compared to the control groups (cell culture media). Moreover, the cultured cells on the hydrogels showed a significant proliferation after 7 days compared to the first and third days showing the potential of the hydrogels for clinical applications. Moreover, the Live/Dead cell viability results (Fig 5F) indicated high cell viability for SF-TA (94.3 ± 2.4 %) and SF-Wool-TA (93.5 ± 3.2 %) without significant difference compared to the control group (97.7 ± 2.4 %) quantified from the fluorescent Live/Dead images (Fig 5G). Furthermore, The cell nucleus staining using Hoechst 33258 (Fig 5H) demonstrated a uniform cell distribution within the hydrogels. The cytocompatibility results indicated that the adhesive hydrogels are a promising candidate for clinical applications such as wound dressing, tissue adhesives, as well as homeostatic materials. Indeed, in addition to the non-toxic nature of SF and wool, the presence of TA may contribute to the cell proliferation and adhesion to the surface of the hydrogels due to the presence of multiple catechol groups, which leads to the interaction with imidazoles or thiols on the cytomembrane of the cell through hydrogen bonding and hydrophobic interaction [25,53,54].

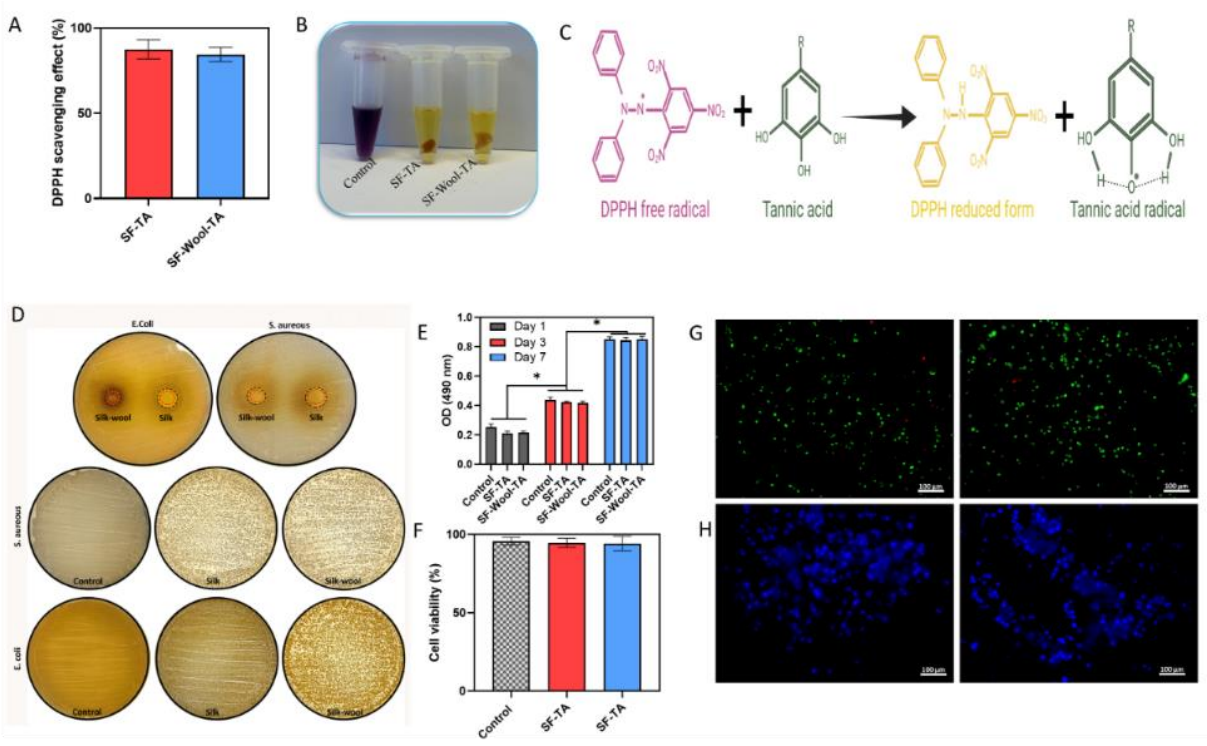

Fig 5. Bioactivity of SF-TA and SF-Wool-TA hydrogels; (A) DPPH scavenging activity of SF-TA and SF-Wool-TA hydrogels; results are expressed as % scavenging activity and are the mean ± SD of three independent experiments. Data were analyzed using a one-way ANOVA test, *$p < 0.05$ as a compared type of hydrogel; (B) SF-TA and SF-Wool-TA hydrogels photographs incubated with DPPH solution for 30 min; (C) Scavenging mechanism of SF-TA and SF-Wool-TA due to the presence of TA molecules; (D) Antibacterial activity of SF-TA and SF-Wool-TA hydrogels using disk diffusion and colony counting assay against E. coli and S. aureus; (E) MTS assay results of 3T3-L1 cell proliferation on the SF-TA and SF-Wool-TA hydrogels after 1, 3, and 7 days of incubation. Results are expressed as optical density (OD) and are the mean ± SD of three independent experiments; (F) 3T3-L1 cell viability after 7 days cultured on the SF-TA and SF-Wool-TA hydrogels quantified from LIVE/DEAD staining, using ImageJ software. Results are expressed as cell viability (%) and are the mean ± SD of three independent experiments. Data were analyzed using a one-way ANOVA test. *$p<0.05$ as a compared type of hydrogel within each time point; (G) Fluorescence microscopic images of Live/Dead staining of 3T3-L1 cell cultured on SF-TA and SF-Wool-TA hydrogels on day 3; (H) Nucleus staining of nucleus staining using Hoechst 33258 showing the cell distribution on the surface of hydrogels.

2.7. Wound healing in a full-thickness skin defect model

The wound-healing potential of adhesive hydrogels was investigated in a full-thickness skin defect model (Fig 6). For this purpose, a circular wound (12 mm full-thickness) was made on the back rat skin and subsequently treated with different materials, including PBS solution (control group), SF-TA, and SF-Wool-TA hydrogel. All the rats survived without infection in the full-thickness wounds. Due to the adhesive property of hydrogels, it could be maintained as an antibacterial and antioxidant wound dress [55]. Gross observations of the wound healing process in a full-thickness skin defect revealed a significant wound closure in SF-TA and SF-Wool-TA hydrogel-treated groups in comparison with the control group after day 14 post-injury (Fig.6 A and B), in which wound diameter was 1.8 ± 0.6 and 2.2 ± 1.0 for the SF-TA and SF-Wool-TA hydrogel -treated vs. 4.9 ± 1.2 mm for the control-treated group (Fig. 6 C). Hence, an enhancement of the wound healing progress by hydrogels was recorded in compared to the control group on day 14 post-injury. The current study results indicated that the control group treatment was not able to promote wound healing. To further investigate wound healing, wound sites were stained with hematoxylin and eosin (H&E) to monitor regenerated skin tissues. No significant

difference was observed in skin photos between the SF-TA and SF-Wool-TA hydrogel-treated groups at any time. H&E staining (Fig. 6D) demonstrated that the SF-TA and SF-Wool-TA hydrogel-treated groups improved re-epithelialization (black arrow) and vascular invasion (yellow arrowhead) in comparison with the control group at day 14. Also, an extensive keratinized layer (black star) as a marker of continuous epithelial cell division and regeneration was observed in SF-TA and SF-Wool-TA hydrogel-treated groups. The wounds treated with SF-TA and SF-Wool-TA hydrogels showed less scar tissue developed (black double-headed arrow) than the control-treated group ($p < 0.05$) (Fig. 1 D). Furthermore, quantification of the scar width demonstrated that the SF-TA and SF-Wool-TA hydrogel-treated groups had a 1710 ± 289 and 1665 ± 345 μm, which is a lower width than the control-treated group (2250 ± 248 μm) (Fig. 1 F). To confirm the efficacy of adhesive hydrogels in skin wound regeneration, sections of wound tissue on day 14 were stained using Masson's trichrome (Fig. 6E). According to Masson's trichrome staining results, a regular arrangement of a wide distribution of collagen fibers (green arrow) was observed in the SF-TA and SF-Wool-TA hydrogel-treated groups. In contrast, collagen fibers (green arrow) showed an irregular and loose arrangement in the control group on days 14 after injury (Fig. 5 E).

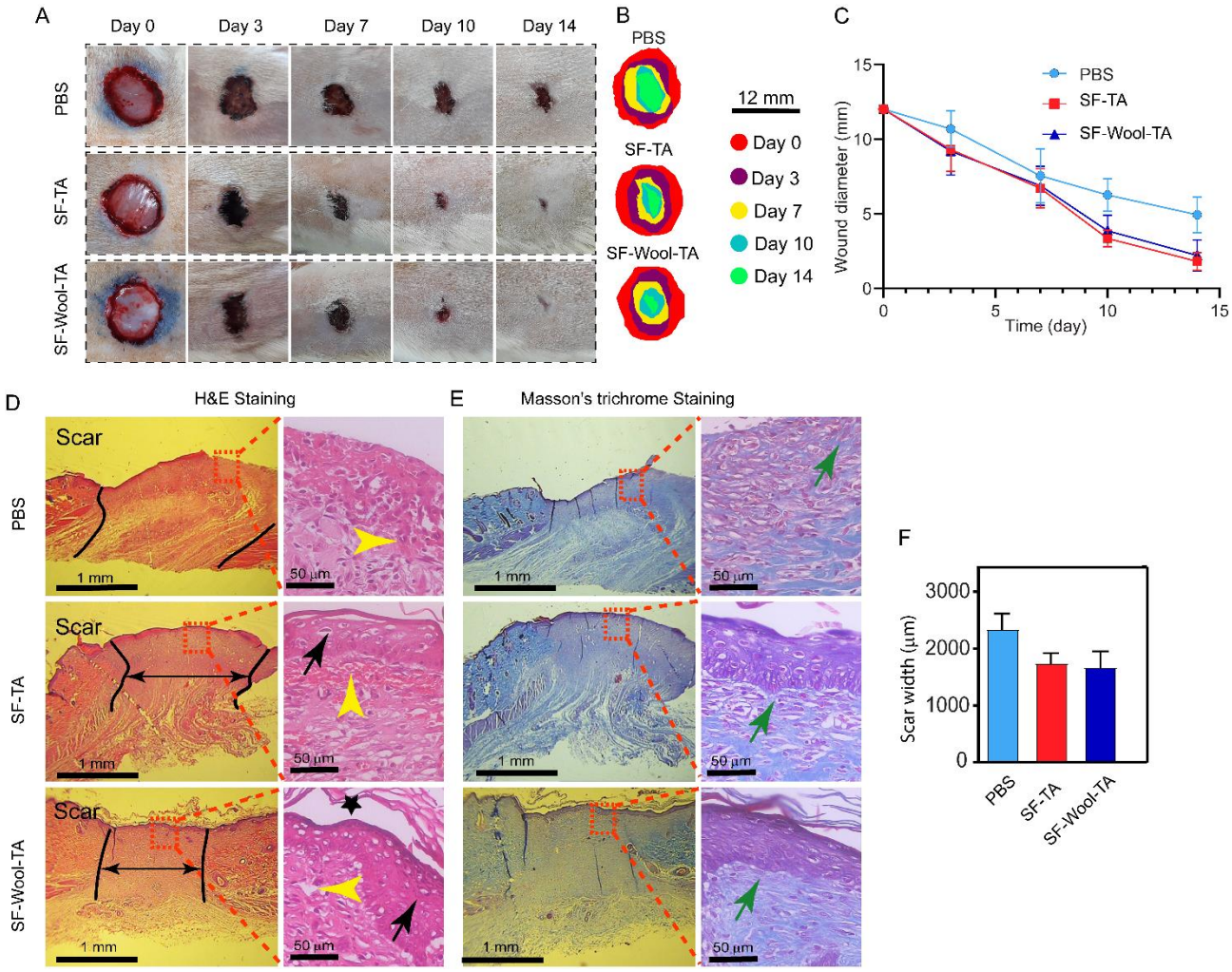

Figure 6. *In vivo* wound healing performance of different treatment adhesive materials and PBS solution (control group), SF-TA, and SF-Wool-TA hydrogels in a full-thickness skin defect model. (A) Hydrogels or PBS were applied to a 12 mm full-thickness skin wound immediately after wounding. Representative photographs of full-thickness skin wound healing *in vivo* in the control-treated group (PBS), the SF-TA, and SF-Wool-TA hydrogel-treated group at 0, 3, 7, 10, and 14 days after injury; (B) Schematic presentation for the wound healing site on the 3, 7, 10 and 14 days after injury; (C) Quantitation of the size of the wound during the wound healing process of each treatment group were determined by analyzing the wound healed in photos; (D) H&E staining images of wound site tissues from different groups. Neo-dermis regeneration outline was marked by black dashed; the scar's width was shown by black double-headed arrows; (E) Masson's trichrome staining of the granulation tissue in control, SF-TA, and SF-Wool-TA hydrogel-treated group on the 14 days of wound healing indicating newly formed collagen fibers distributed into the granulation tissue; (F) Quantitation of the scar width (black double-headed arrows in d) of different groups after 14 days of injury. Rats, n = 5. Statistical significance was

analyzed by one-way ANOVA followed by a Tukey post hoc analysis between multiple groups, and statistical significance was considered as *$p < 0.05$. Data are shown as the mean ± standard deviation.

2.8. Wound closure evaluation of full-thickness skin incision

A full-thickness skin incision model was employed to assess the efficacy of adhesive hydrogels in promoting wound closure. Two-centimeter-long full-thickness skin incisions were created on the dorsal region of rats and treated with surgical sutures, SF-TA hydrogel, SF-Wool-TA hydrogel, or left untreated as a control (PBS). The results, depicted in Figure 7A, revealed that during the initial stages of wound healing, the control group and both hydrogel-treated groups experienced an increase in incision size due to animal movement, while the incisions treated with surgical sutures remained closed. The hydrogel exhibited flexibility and exhibited adhesion to the incision site without displacement (Video S5). By day 14, the incisions in the surgical suture and adhesive hydrogel groups were almost healed, whereas visible incisions persisted in the control groups. Although slight scarring was observed in the SF-TA and SF-Wool-TA hydrogel groups, the structure of the healing tissue differed in the suture group (Fig. 7A). Consequently, treatment with either surgical sutures or adhesive hydrogels facilitated early wound closure and accelerated the healing process. To further evaluate wound healing, histological analysis using HE and Masson trichrome staining was performed on day 14. As shown in Figure 7B, the control group exhibited incomplete formation of the epidermis and subcutaneous tissues due to wound disruption. In contrast, the surgical suture and adhesive hydrogel groups displayed fully healed epidermis and subcutaneous tissues. Although wound fissures were still observable in all treatment groups, they were not as pronounced as in the control group. Moreover, compared to the control group, the surgical suture and adhesive hydrogel groups exhibited improved healing effects. Masson trichrome staining results indicated enhanced collagen deposition in the surgical suture and adhesive hydrogel groups compared to the control group. Notably, the SF-Wool-TA hydrogel demonstrated denser collagen fiber and more organized collagen deposition in the healed tissues compared to other groups. This data underscores the superior adhesive properties of the hydrogel, which facilitate effective incision closure, and highlights its beneficial antioxidant and antibacterial properties, contributing to accelerated wound healing after closure. Figure 7C presents the proposed model

elucidating the wound healing mechanism of SF-Wool-TA adhesive hydrogel. The release of tannic acid from the SF-Wool-TA hydrogel may prevent bacterial infection due to its potent antibacterial activity, while its antioxidant activity can mitigate oxidative stress and safeguard cells against free radical-induced damage. Additionally, the presence of wool keratin may stimulate the growth and migration of key cells involved in the wound-healing process, such as fibroblasts and keratinocytes.

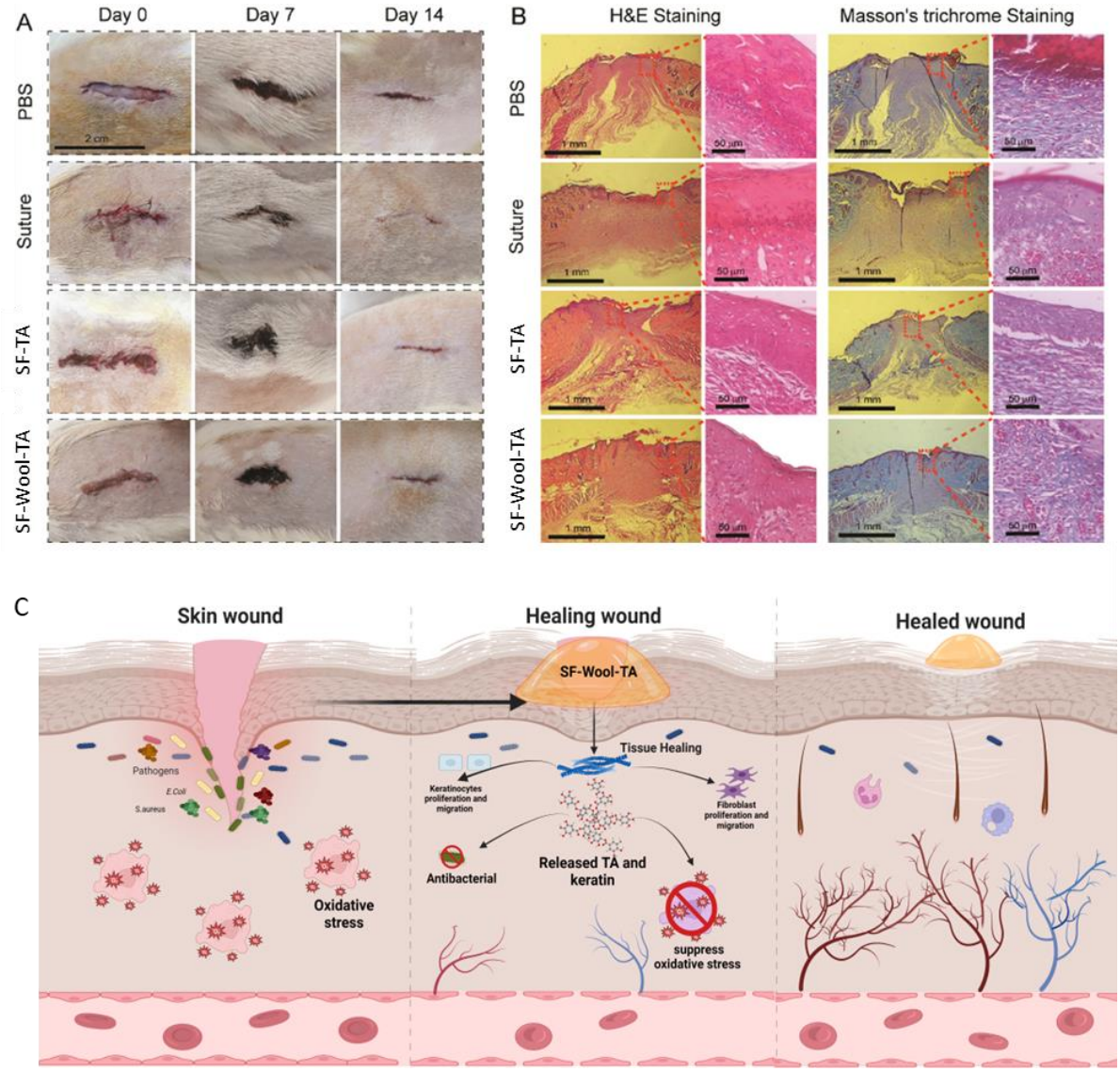

Figure 7. Wound closure evaluation of different treatment adhesive materials a) photograph of skin incision modeling and treatments, representative images of the incisional skin wounds treated by surgical sutures,

Hydrogel, and Hydrogel-Wool, as well as the skin incisions without treatment (PBS solution) at determined times; B) H&E stained and Masson's trichrome stained images of skin incisions after healed for 14 days. Rats, n = 5. Statistical significance was analyzed by one-way ANOVA followed by a Tukey post hoc analysis between multiple groups, and statistical significance was considered as *$p < 0.05$. Data are shown as the mean ± standard deviation; C) Schematic illustration for the mechanism of wound healing using the SF-Wool-TA adhesive hydrogel.

3. Conclusion

The formation of adhesive hydrogels through the synergistic non-covalent interactions between silk fibroin (SF), wool keratin, and tannic acid (TA) has been demonstrated. The resulting hydrogels indicated a three-dimensional porous microstructure, self-gelling features, and high adhesive properties to the biological tissue. The presence of TA molecules in the hydrogels led to a high antioxidant and antibacterial activity, which is essential for wound healing applications. Moreover, the hydrogels showed non-toxicity and cytocompatibility, which supports their potential for clinical applications. The SF-Wool-TA has potential applications in wound healing due to its self-gelling property, high water uptake, and retention, which can improve re-epithelialization rate by facilitating epithelial cell movement, and hemostasis rate by enhancing wound exudate absorption.

4. Materials and methods

4.1. Materials

Bombyx mori cocoons were purchased from Dropshipping C Store, Aliexpress. Raw waste coarse wool, free from coarse fertilizer and litter, was locally sourced. Sodium carbonate (Na_2CO_3), lithium bromide (LiBr), 2,2-Diphenyl-1-picrylhydrazyl (DPPH), Hoechst (H33342), ethidium homodimer I (E1903) were purchased from Sigma-Aldrich (St. Louis, MO, USA). Tannic acid, 95%, was purchased from Acros Organics (NJ, USA).

4.2. Preparation of wool keratin and silk fibroin

The wool keratin was prepared using microwave (MW) treatment according to our previous study [56]. Silk fibroin (SF) solution was prepared from *B. mori cocoons*, based on our previous study [57]. Details are described in ESI note 1.

4.3. Synthesis of SF-Wool-TA adhesive hydrogel

The SF-Wool-TA was prepared by simply mixing protein mixture (SF-Wool) with TA solution. Briefly, 500 mg wool keratin was added to 10 mL SF solution (5 %) and vortexed to ensure the complete dispersion of wool keratin. Then, the TA solution (30 %) was added to the SF-Wool with a volume ratio of 2:1 (TA: SF-Wool). The adhesive SF-Wool-TA gel was obtained after centrifugation and removing unreacted TA by mild washing process with water (3 times). The adhesive SF-Wool-TA gel was freeze-dried and powdered for all the experiments. A hydrogel without wool keratin (SF-TA) was prepared as a control.

4.4. Adhesive hydrogels characterization

The hydrogel physiochemical properties were investigated, such as chemical composition by FT-IR, crystallinity using XRD, initial water content (IWC), gel content, swelling behavior, and hydrogels' water retention. Details are described in the ESI note 2.

4.5. Rheological and adhesion properties of the adhesive hydrogels

The viscoelastic properties of the adhesive hydrogels were determined using a rheometer (Anton Paar MCR 302, Austria) equipped with a plate-plate geometry (25 mm) at 37 °C. To assess the adhesion properties of SF-Wool-TA adhesive, a lap shear test was performed using a Zwick/Roell Z020 universal testing machine (Zwick GmbH, Ulm, Germany) according to a previously described method [33]. Details are described in the ESI note 3.

4.6. TA release from the adhesive hydrogels

TA release rate from the adhesive hydrogels was investigated according to a previously described method [40]. Details are described in the ESI note 4.

4.7. Antioxidant activity and antibacterial properties of the adhesive hydrogels

The antioxidant activity of adhesive hydrogels was determined using a DPPH scavenging assay [58]. The antibacterial activity of adhesive hydrogels was investigated against *S. aureus* (Gram-positive) and *E.coli* (Gram-negative) by using colony counting and disk diffusion assay [40]. Details are described in ESI note 5.

4.8. Cytocompatibility of hydrogels

The toxicity of adhesive hydrogels was determined using 3T3-L1 mouse fibroblast cells via Live/Dead and MTS assay [59]. Details are described in the ESI note 6.

4.9. Animal care and surgical procedure

The study used male Sprague Dawley rats (n=42) that weighed between 250-300 g and were acquired from the Laboratory of Animals Breeding Center at Shiraz University of Medical Sciences in Iran. The ethical guidelines of Shiraz University of Medical Sciences (Shiraz, Iran) were followed, and the study was approved by its ethics committee. (Approval ID: IR.SUMS.AEC.1401.132).

4.10. Evaluation of hydrogel for regeneration of infected full-thickness skin wound:

The in vivo wound healing potential of the hydrogels was evaluated using a full-thickness acute wound model according to our previous study [60]. The study used male Sprague Dawley rats (n=42) that weighed between 250-300 g and were acquired from the Laboratory of Animals Breeding Center at Shiraz University of Medical Sciences in Iran. The ethical guidelines of Shiraz University of Medical Sciences (Shiraz, Iran) were followed, and the study was approved by its ethics committee. (Approval ID: IR.SUMS.AEC.1401.132). Details are described in the ESI note 7.

4.11.Evaluation of the hydrogel on skin scratch healing

For the mouse skin incision model, a wound closure assay was carried out based on the existing literature with some modifications [61]. Details are described in the ESI note 8.

4.12. Histology analysis

Hematoxylin-eosin (H&E) and Masson's trichrome staining were performed after 14 days to investigate the histology analysis of the newly formed skin tissues. Details are described in the ESI note 9.

4.13. Statistical analysis

The results were presented as means ± standard deviations. The statistical analysis was performed by applying one-way ANOVA, followed by Tukey's post-hoc analysis. P-values less than 0.05 were considered statistically significant and indicated by *$p < 0.05$ whenever significance was proven.

Declaration of Competing Interest

The authors declare no conflict of interest.

Acknowledgments

H.J and A.S. acknowledge funding from Innoviris Brussels, Belgium (https://innoviris.brussels) under the project 2019 – BRIDGE – 4: RE4BRU. The content is solely the authors' responsibility and does not necessarily represent the official views of the above-mentioned funding agency. A.S. acknowledge the support of Wallonie-Bruxelles International (WBI) (CMP W-B/Quebec 2022-2024-confirmation WBI SUB/2023/591790). HS is grateful for the support of the Natural Sciences and Engineering Research Council of Canada (NSERC) (NSERC, RGPIN-2021-03960, DGECR-2021-00337), Fonds de Recherche du Québec Santé (FRQS) (Chercheurs-boursiers J1 (313837)), Establishment of Young Investigators (324277), Montreal TransMedTech Institute (iTMT), CRCHU Sainte Justine (CRCHUSJ), and University of Montreal. AM and HS greatly appreciate the support from the bilateral cooperation program between Québec–Wallonia-Brussels (12ème CMP W-B/Québec 2022-2024). The authors would like to thank Dr. Véronique Fontaine and Dr. Christine Delporte for their assistance with the antibacterial and cell viability analysis and Dr. Bernaert's assistance with the lap shear test experiment.

Data availability

The raw/processed data required to reproduce these findings cannot be shared at this time as the data also forms part of an ongoing study.

References

1. Zhu, Z*., et al.*, Valorization of waste and by-products from food industries through the use of innovative technologies. In *Agri-Food Industry Strategies for Healthy Diets and Sustainability*, Elsevier(2020), pp 249
2. Biswal, T*., et al.*, *Materials Today: Proceedings* (2020)
3. Liu, X*., et al.*, *Materials Science and Engineering: C* (2019) **99**, 1509
4. Rajabi, M*., et al.*, *Materials Science and Engineering: C* (2020) **110**, 110612
5. Feroz, S*., et al.*, *Bioactive Materials* (2020) **5** (3), 496
6. Cascone, S., and Lamberti, G., *International Journal of Pharmaceutics* (2020) **573**, 118803
7. Taboada, G. M*., et al.*, *Nature Reviews Materials* (2020) **5** (4), 310
8. Owens, C., and Stoessel, K., *Journal of hospital infection* (2008) **70**, 3
9. Matossian, C*., et al.*, *Clinical Ophthalmology (Auckland, NZ)* (2015) **9**, 921
10. Luo, J*., et al.*, *Advanced Healthcare Materials* (2020) **9** (4), 1901423
11. Liao, M*., et al.*, *Advanced Functional Materials* (2017) **27** (48), 1703852
12. Peng, X*., et al.*, *Advanced Functional Materials* (2021) **31** (33), 2102583
13. Coover, H., *J Soc Plast Eng* (1959) **15**, 413
14. Tan, H*., et al.*, *Biomaterials* (2019) **192**, 392
15. Rai, R*., et al.*, *Progress in polymer science* (2012) **37** (8), 1051
16. Grunzweig, K. A*., et al.*, *Journal of Plastic, Reconstructive & Aesthetic Surgery* (2019) **72** (6), 871
17. Chen, T*., et al.*, *Journal of Biomedical Materials Research Part B: Applied Biomaterials: An Official Journal of The Society for Biomaterials, The Japanese Society for Biomaterials, and The Australian Society for Biomaterials and the Korean Society for Biomaterials* (2006) **77** (2), 416
18. Jalalvandi, E., and Shavandi, A., *Journal of the Mechanical Behavior of Biomedical Materials* (2019) **90**, 191
19. Nam, S., and Mooney, D., *Chemical Reviews* (2021) **121** (18), 11336
20. Costa, F*., et al.*, *Peptides and proteins as biomaterials for tissue regeneration and repair* (2018), 175
21. Boni, R*., et al.*, *Journal of Materials Science: Materials in Medicine* (2020) **31** (9), 1
22. Ghaffari-Bohlouli, P*., et al.*, *Critical reviews in food science and nutrition* (2022), 1
23. Jing, Y*., et al.*, *Biomaterials Advances* (2023) **149**, 213405
24. Gao, X*., et al.*, *Biomaterials science* (2020) **8** (9), 2694
25. Chaudhuri, O*., et al.*, *Nature* (2020) **584** (7822), 535
26. Zheng, H*., et al.*, *Chemical Engineering Journal* (2022), 136931
27. Spencer, C. M*., et al.*, *Phytochemistry* (1988) **27** (8), 2397
28. Bai, S*., et al.*, *Nanoscale Horizons* (2019) **4** (6), 1333
29. Ranjit, E*., et al.*, *Journal of Science: Advanced Materials and Devices* (2021)
30. Ren, Y*., et al.*, *Journal of Photochemistry and Photobiology B: Biology* (2020) **202**, 111676
31. Jing, J*., et al.*, *ACS Biomaterials Science & Engineering* (2019) **5** (9), 4601
32. Peng, X*., et al.*, *Science Advances* (2021) **7** (23), eabe8739
33. Jafari, H*., et al.*, *Carbohydrate Polymers* (2022), 119844
34. Shavandi, A*., et al.*, *Green chemistry* (2021) **23** (3), 1171
35. Okoro, O. V*., et al.*, *Chemical Papers* (2022) **76** (5), 2637
36. Wang, K*., et al.*, *Green Chemistry* (2016) **18** (2), 476
37. Jafari, H*., et al.*, *ACS Biomaterials Science & Engineering* (2018) **4** (7), 2484
38. Zhu, H*., et al.*, *European Polymer Journal* (2017) **86**, 154

39. Ninan, N.*, et al.*, *ACS applied materials & interfaces* (2016) **8** (42), 28511
40. Ahmadian, Z.*, et al.*, *Advanced healthcare materials* (2021) **10** (3), 2001122
41. Wu, P.*, et al.*, *International journal of biological macromolecules* (2018) **114**, 1168
42. Wang, Y.*, et al.*, *Journal of Applied Polymer Science* (2021) **138** (7), 49862
43. Mir, M.*, et al.*, *Progress in biomaterials* (2018) **7** (1), 1
44. Zandi, N.*, et al.*, *Biomaterials* (2021) **267**, 120476
45. Yu, A. C.*, et al.*, *Nature communications* (2021) **12** (1), 1
46. Jafari, H.*, et al.*, *Journal of Materials Chemistry B* (2022)
47. Cheng, Z.*, et al.*, *Regenerative Biomaterials* (2021) **8** (2), rbab008
48. Sando, L.*, et al.*, *Journal of Biomedical Materials Research Part A* (2010) **95** (3), 901
49. Selvaraj, S., and Fathima, N. N., *ACS applied materials & interfaces* (2017) **9** (7), 5916
50. Azadikhah, F.*, et al.*, *International Journal of Biological Macromolecules* (2021) **188**, 114
51. Li, S.*, et al.*, *Advanced science* (2018) **5** (5), 1700527
52. Wang, S.*, et al.*, *Surface and Coatings Technology* (2007) **202** (3), 460
53. Chang, M.*, et al.*, *Journal of Materials Science* (2021) **56** (26), 14729
54. Meng, Z.*, et al.*, *ACS Applied Bio Materials* (2021) **4** (3), 2713
55. Guo, S.*, et al.*, *Advanced Healthcare Materials* (2022) **11** (4), 2101808
56. Shavandi, A., and Ali, A., *Journal of environmental chemical engineering* (2018) **6** (5), 6700
57. Jafari, H.*, et al.*, *Gels* (2021) **7** (3), 138
58. Jafari, H.*, et al.*, *Green Chemistry* (2022) **24** (6), 2409
59. Jafari, H.*, et al.*, *Carbohydrate polymers* (2022) **295**, 119844
60. Jafari, H.*, et al.*, *Applied Materials Today* (2022) **29**, 101581
61. Akhramez, S.*, et al.*, *Sustainability (Switzerland)* (2022) **14** (14)